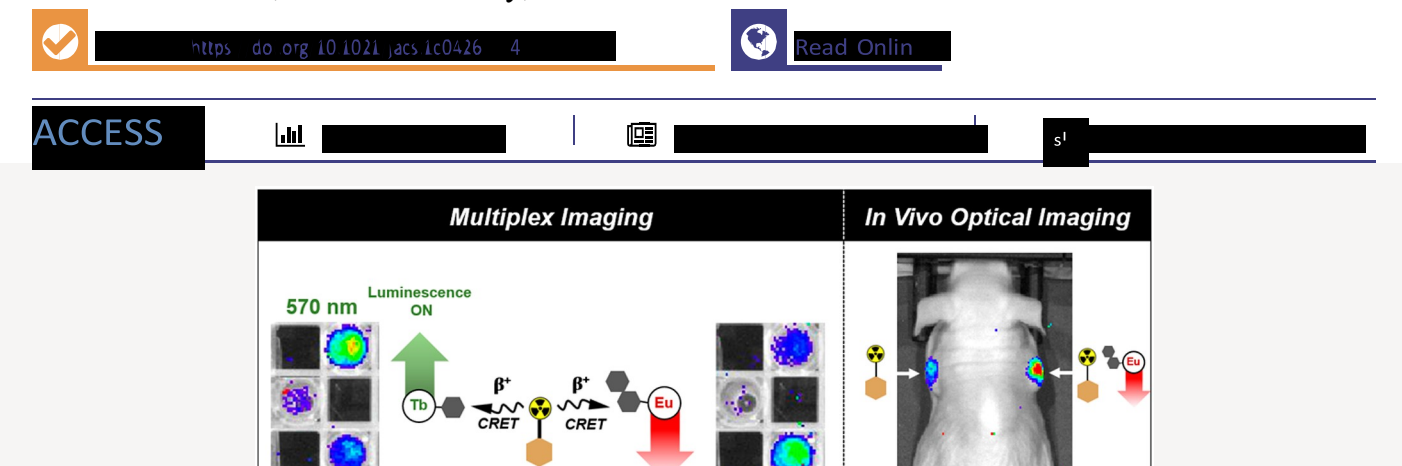


pubs.acs.org/JACS \_\_\_\_Article

# Multiplex and In Vivo Optical Imaging of Discrete Luminescent Lanthanide Complexes Enabled by In Situ Cherenkov Radiation Mediated Energy Transfer

Kirsten E. Martin, Alexia G. Cosby, and Eszter Boros\*



620 nm

ABSTRACT:

INTRODUCTION

thus allow efficient energy transfer with excitation wavelengths of 250–350 nm. This complicates bioimaging applications, as short-wavelength excitation light has very limited tissue depth penetration. owing

produces narrow emission bands independent of the metal coordinative environment, (ii) long luminescence lifetimes, and (iii) diminished photobleaching and self-quenching effects.<sup>1,2</sup> Emission maxima vary depending on the lanthanide, such as Tb(III), which emits green ( $\lambda_{em} = 490$ , 545 nm), or Eu(III), which emits red ( $\lambda_{em} = 613$ , 690 nm).<sup>3</sup>

Despite the advantages of lanthanide luminescence emission<sup>4</sup> and its increasingly widespread application in bioassays, lanthanide complexes have remained underexplored

luminescent lanthanide complexes, we have introduced the

application of Cherenkov radiation (CR) as an in situ excitation source. Radioisotopes that meet the energy requirement to generate CR, such as positron emitters <sup>18</sup>F or <sup>89</sup>Zr, <sup>9</sup> provide an alternative source of short-wavelength light for lanthanide excitation. <sup>10,11</sup> CR in aqueous solutions is continuous, and its intensity exhibits a  $1/\lambda^2$  dependence. As a consequence, intensity is significantly enhanced below 400 nm, which correlates well with the ideal excitation wavelengths

for bioimaging applications beyond cell assays and the imaging of translucent, multicellular organisms. 5.6 Due to the Laporteforbidden nature of the 4f-f transitions, excitation of aromatic chromophores ("antennas") followed by intersystem crossing and energy transfer is typically required to access lanthanide luminescence. 7.8 The antenna must possess a triplet state energy that is comparable to lanthanide acceptor states and

Received:

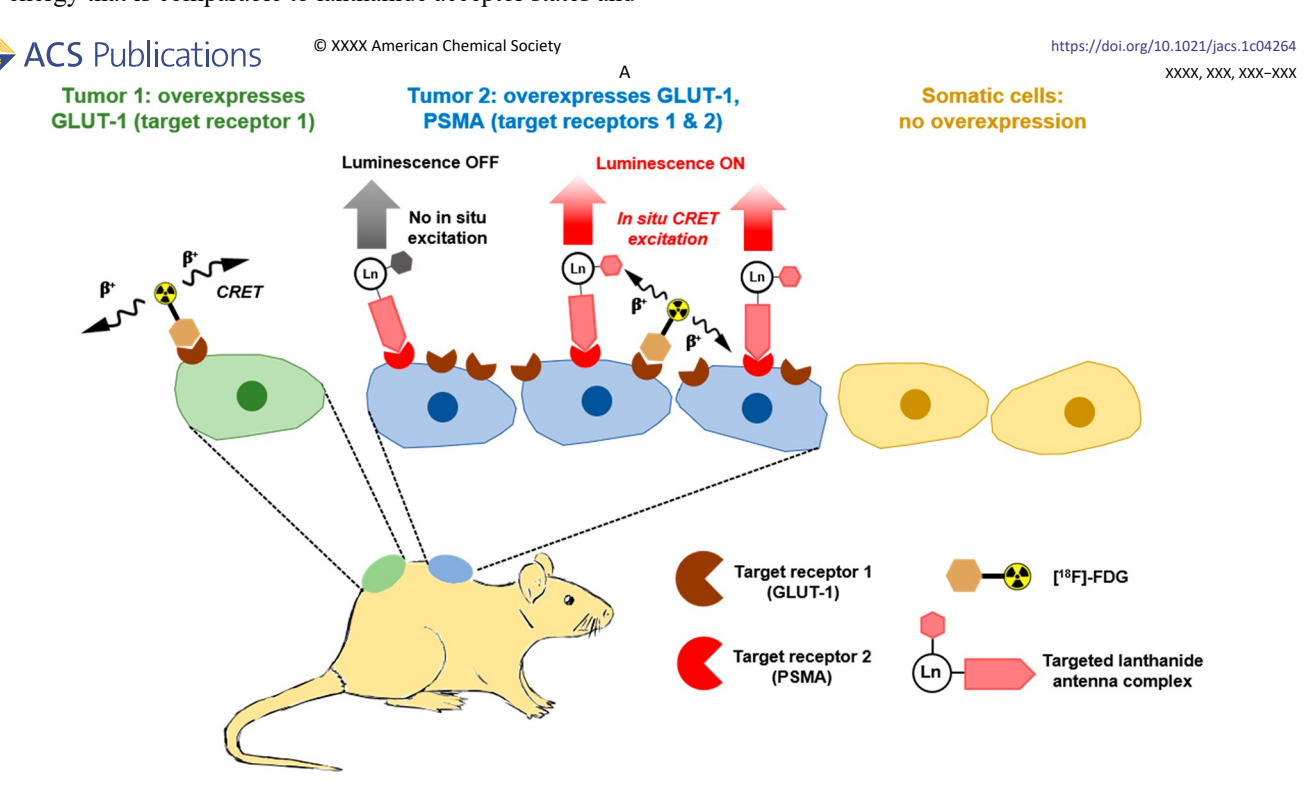


Figure 1. Schematic depiction of the in situ CRET-mediated excitation of discrete, targeted Ln(III) complexes. Specifically, we propose to use the clinically employed PET agent [<sup>18</sup>F]-FDG as a CRET source that exhibits uptake in cancer cells broadly due to the overexpression of GLUT-1 transporters. Here, we propose that discrete luminescent lanthanide complexes functionalized with a targeting vector that is only expressed in a subpopulation of cancer cells can be used to selectively illuminate these cells when colocalized with the CR source. The in situ excitation of these probes enables wavelength selective multiplex imaging and the detection of long wave emission of Ln(III) complexes with conventional optical imaging tools, obviating the need for high intensity laser excitation sources or time-resolved luminescence detection.

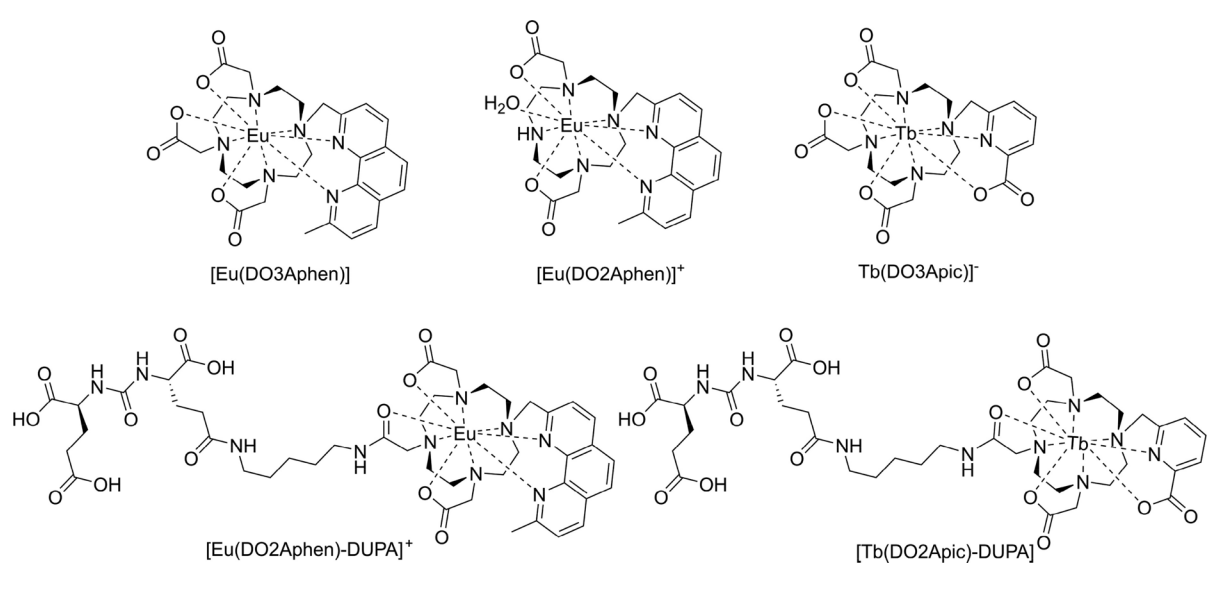


Figure 2. Complexes explored in this work.

of lanthanide antennas. 12-14 We have successfully established CRET as a means to excite discrete luminescent lanthanide complexes and employ CRET excitation to estimate quantum yields of Tb(III) complexes in a high-throughput manner. 15,16 Motivated by our results, we posited that functionalized, high quantum yield Tb(III) and Eu(III) complexes bore potential for multiplexed and even targeted in vivo optical imaging when combined with a CR-emissive positron emission tomography (PET) radiopharmaceutical (Figure 1). The latter has been widely regarded as not feasible without specialized means of excitation such as twophoton excitation/upconversion and custom-built laser photon sources<sup>6,17</sup> and even if enabled, is further complicated by the need of exceedingly large quantities of lanthanide ion to produce a detectable luminescence signal. Indeed, the in situ excitation and in vivo imaging of luminescent quantum dots with CRET have been reported, but nanoparticles typically govern biological behavior and exhibit characteristic off-target uptake in the spleen, lungs, or liver. 18,19 Discrete molecular systems do not suffer from this predicament, yet have widely been considered not suitable to produce signal above the limit of detection even when compound quantities in the µmol range are employed.

Here, we demonstrate the feasibility of multiplexed imaging with discrete, luminescent Tb(III)- and Eu(III)-based imaging probes with optimized optical properties using conventional optical imaging equipment. We also probed the compatibility of these probes for in vivo imaging in conjunction with the widely clinically available PET tracer [18F]-fluorodeoxyglucose (FDG) and show that targeted Eu(III) probes can produce a persistent emission signal in mouse tumor xenografts in vivo and ex vivo.

## RESULTS AND DISCUSSION

Ligand Design and Complex Synthesis of Eu(III)

Chelates. Our first challenge represented the synthesis of an Eu(III) chelate with suitable optical and robust chemical properties to withstand implementation of bioconjugation. On the basis of our work on the CRET mediated excitation of Tb(III), complexes with quantum yields below 10% were not deemed suitable. 15,16 Competing, nonradiative deexcitation processes result in considerably lower quantum yields of Eu(III) complexes when compared with their Tb(III) analogues. While heteroarylalkyne linked antennas have been used extensively to produce inert, high quantum yield Eu(III) complexes suitable for time-resolved in vitro imaging, <sup>20-24</sup> the diminished solubility and incompatibility with acidic deprotection conditions commonly employed for orthogonal peptide conjugation chemistry were not desirable for our particular applications. Efficient energy transfer from the antenna T<sub>1</sub> to the <sup>5</sup>D<sub>1</sub> Eu(III) excited state requires a T<sub>1</sub> energy of >22 000 cm<sup>-1</sup> to enable efficient energy transfer to <sup>5</sup>D<sub>1</sub> at 19 000 cm<sup>-1</sup>. <sup>25</sup> Following the work of Quici et al, we synthesized a tetraazamacrocyclic-based chelator containing

a phenanthroline antenna (DO3Aphen, Figure 2), which had been identified to produce robust  $\Phi_{Ln}$  of >20%.<sup>26</sup>

Chemical synthesis was achieved following previously published procedures.<sup>26,28</sup> In short, commercially available was used synthesize dimethylphenanthroline to acetoxymethylphenathroline in two steps, which was deacetylated under basic conditions and mesylated for subsequent alkylation to DO3AtBu<sup>29</sup> (Scheme S1). Removal of the tert-butyl protecting groups under acidic conditions yields DO3Aphen, which was complexed with a europium triflate salt in water, by increasing the pH to between 7 and 7.5 with 0.1 M NaOH. Complex formation was monitored by analytical HPLC and observation of the characteristic europium-based red emission of the resulting complex [Eu(DO3Aphen)]. To probe the sensitivity of europium complexes to O-H mediated de-excitation, a monohydrated complex analogue [Eu(DO2Aphen)]+ was also synthesized in analogous manner to [Eu(DO3Aphen)] using the protected macrocycle DO2A-tBu<sup>30</sup> for alkylation, which was then deprotected under acidic conditions and complexed as described above (Scheme S2). We determined inner-sphere hydration number (q) of both complexes using Horrocks' equations and employed the established gradient-based method to determine quantum yield. <sup>27,31,32</sup> [Eu(DO3Aphen)] was confirmed to be a q = 0 complex and possesses a moderate quantum yield of 15%. The [Eu(DO2Aphen)]<sup>+</sup> complex was confirmed to be a q = 1 complex and, correspondingly, possesses a decreased quantum yield of 5%. This significant decrease in quantum yield highlights the necessity for europium complexes to efficiently exclude inner-sphere hydration for viable applications in the context of CRET imaging (Table 1).

Table 1. Photophysical Characterization Including Gradient-Based QY ( $\Phi_{Ln}$ ), Inner-Sphere Hydration Number (q), and Luminescent Lifetimes ( $\tau$ ) Determined in H<sub>2</sub>O or D<sub>2</sub>O

complex	Ф <sub>Lna</sub> (%)	$\tau$ , H <sub>2</sub> O (ms)	$\tau$ , $D_2O$ (ms)	qь
[Eu(DO3Aphen)]	15	1.27	1.79	0
[Eu(DO2Aphen)] <sup>+</sup>	5	0.58	1.82	1.11
[Eu(DO2Aphen)-DUPA] <sup>+</sup>	10	1.17	1.73	0
[Tb(DO3Apic)] <sup>-15</sup>	47	2.83	2.75	0
[Tb(DO2Apic)-DUPA]	38	1.09	1.13	0

 $_{a}$  Reported with an error of  $\pm 10$ –15%.  $_{b}$  Reported with an error of  $\pm 20\%.^{27}$ 

The kinetic inertness [Eu(DO3Aphen)] and [Tb(DO3Apic)] investigated was diethylenetriaminepentaacetic acid (DTPA) challenge.33-35 In presence of 1000× excess DTPA in Dulbecco's phosphate buffered saline (DPBS, pH 7.4), the antenna absorption peak of [Eu(DO3Aphen)] remained centered at 285 nm (characteristic of complex) rather than 275 nm (characteristic of unchelated ligand), indicating no transchelation occurred over 14 days. Additionally, the retention time of the samples remained consistent with that of the complex (t<sub>R</sub> complex, 5.02 min; t<sub>R</sub> ligand, 4.85 min), further affirming that the DO3Aphen scaffold was sufficiently inert for prospective biological applications (Figures S53–S55). [Tb(DO3Apic)]

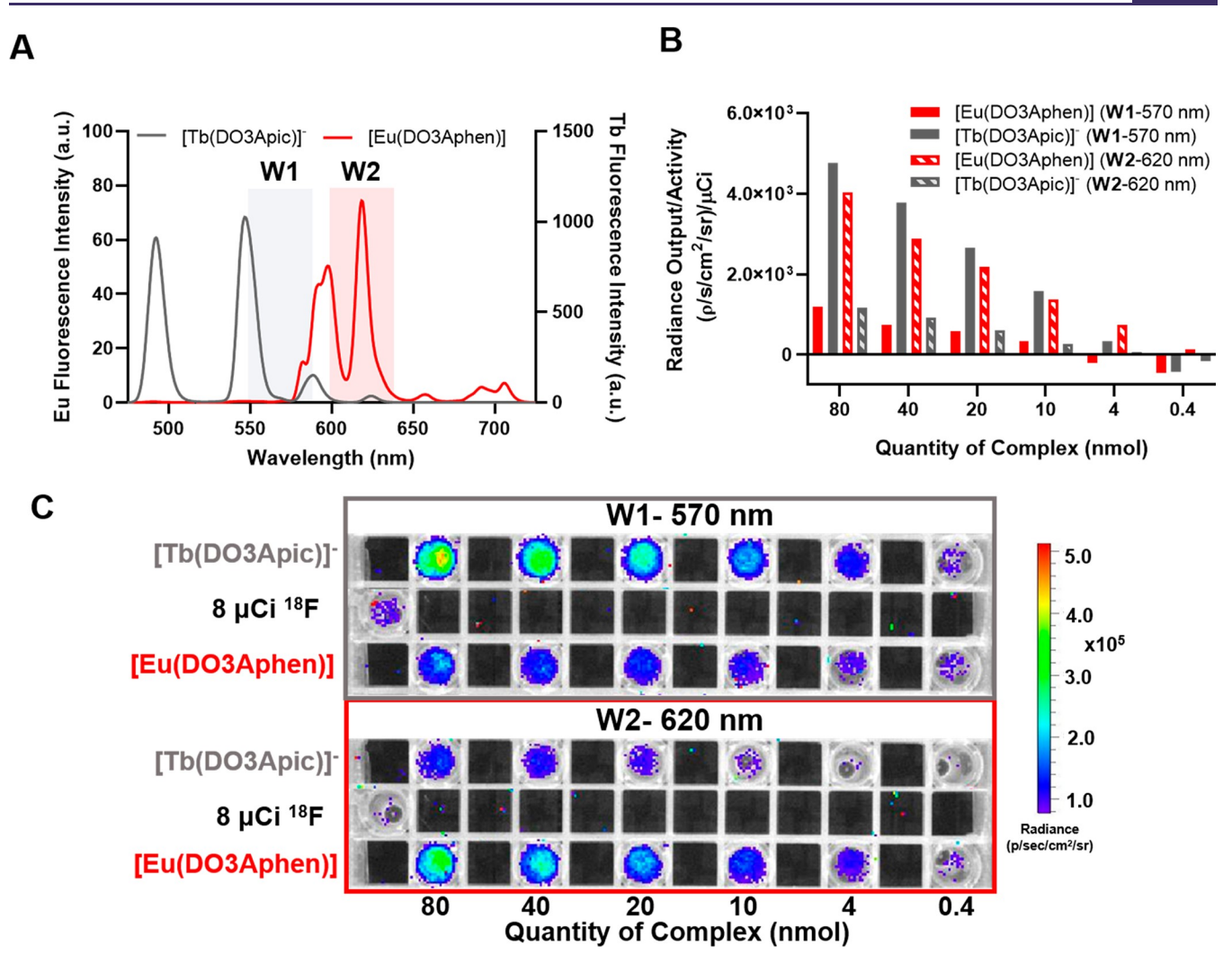


Figure 4. Multiplexed imaging of nonfunctionalized complexes: (A) emission filter windows (W1, 570 nm; W2, 620 nm) overlaid with the luminescence spectra of [Eu(DO3Aphen)] and [Tb(DO3Apic)]<sup>-</sup>; (B) quantified radiance of the complexes in the presence of 8  $\mu$ Ci of Na<sup>18</sup>F using region of interest analysis; (C) phantom images of the nonfunctionalized complexes with emission filters (W1 and W2) in the presence of 8  $\mu$ Ci of Na<sup>18</sup>F.

exhibited comparable kinetic stability under identical conditions (Figures S56–S58). Identical results were produced at pH 6.5, indicating that the complexes were sufficiently inert under conditions mimicking acidic tumor microenvironments (Figures S59 and S60).

Optical Imaging of Eu(III) Complexes Using CRET Excitation. To assess the suitability of newly synthesized Eu(III) complexes and determine appropriate functionalization strategies, we evaluated the CRET-mediated excitation of the nonfunctionalized model complexes using optical imaging of phantoms containing 10  $\mu$ Ci of Na<sup>18</sup>F. We selected this quantity of radioactivity as this is a typical quantity of activity used in in vivo PET imaging.<sup>36,37</sup>

Solutions of 1–150 nmol of [Eu(DO3Aphen)] and [Eu(DO2Aphen)]<sup>+</sup> in DPBS were doped with 8  $\mu$ Ci of Na<sup>18</sup>F and imaged on a conventional small animal scanner, with blocked excitation and emission collected from 500 to 845 nm (Figure 3). Region of interest (ROI) analysis revealed

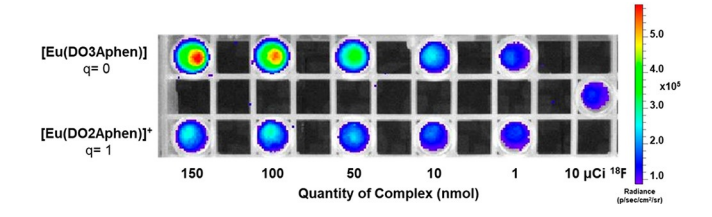


Figure 3. CRET excitation of [Eu(DO3Aphen)] and [Eu(DO2Aphen)] showing the impact of hydration on radiance output.

increased signal intensity of [Eu(DO3Aphen)] compared to [Eu(DO2Aphen)]<sup>+</sup>, a result in accordance with their respective quantum yields: significant decrease in radiance was observed for the [Eu(DO2Aphen)]<sup>+</sup> complex (Figure S63). Radiance of [Eu(DO3Aphen)] could be detected with a limit of detection (LOD) of 10 nmol of complex, while [Eu(DO2Aphen)]<sup>+</sup> possessed a significantly increased limit of detection of 50

nmol underscoring that quantum yields of at least 10% are required for the detection of biologically relevant optical probe compound concentrations.

Multiplex Optical Imaging. The differential optical emission properties of the Eu(III) and Tb(III) complexes enable detection at different wavelengths of emission (Figure 4A). To validate this concept, we carried out CRET imaging experiments with the nonfunctionalized Eu(III) and Tb(III) complexes. The previously studied [Tb(DO3Apic)]-complex was synthesized as described<sup>15</sup> and solutions of 0.4–80 nmol of [Eu(DO3Aphen)] and [Tb(DO3Apic)]- in DPBS were doped with 10 μCi of Na<sup>18</sup>F and imaged (Figure 4C). Emission of the two complexes was observed using 40 nm bandpass emission filters centered at 570 and 620 nm. Region of interest (ROI) analysis (Figure 4B) revealed that for complex quantities of 10 nmol with imaging centered at 570 nm, emission of [Tb(DO3Apic)]- was 4.6× greater than

that of [Eu(DO3Aphen)]. At the same concentration with wavelength detection centered at 620 nm, emission of [Eu(DO3Aphen)] was 5.3× greater than that of [Tb(DO3Apic)]<sup>-</sup>. Discernable, wavelength selective emission was detected with probe as little as 4 nmol. This initial proof-of-concept study validates the feasibility of multiplexed optical imaging using Eu(III) and Tb(III) complexes and can enable the simultaneous imaging of two targets without the need for time-resolved spectral deconvolution.<sup>5,38</sup>

Synthesis of Targeted Peptide Conjugates. To assess the use of discrete Tb(III) and Eu(III) complexes for targeted applications, conjugated versions of model complexes were synthesized. The phenanthroline-based system was functionalized using the linker-functionalized dipeptide, 2-[3-(1,3dicarboxypropyl)ureido]pentanedioic acid (DUPA). DUPA targets the prostate-specific membrane antigen

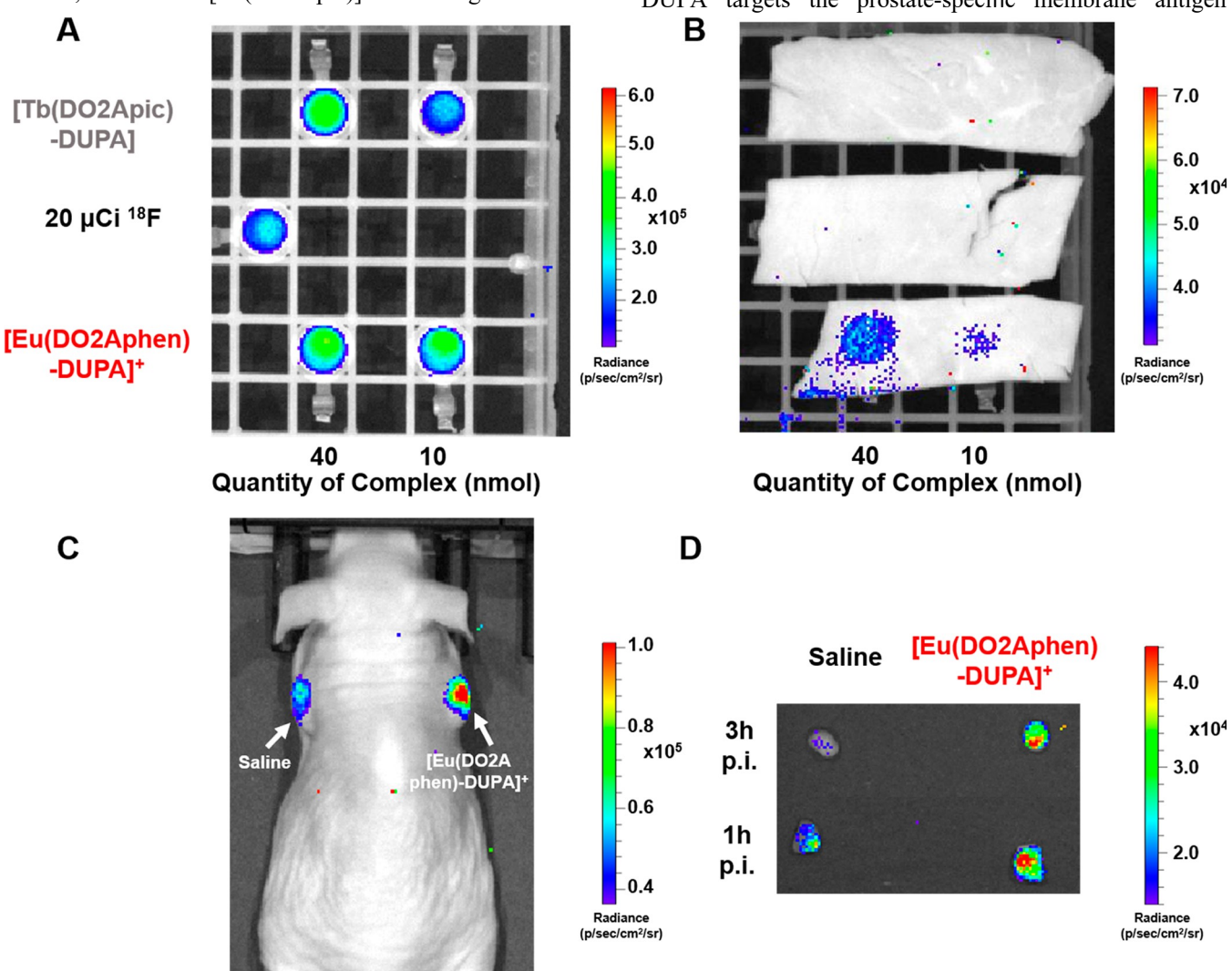


Figure 5. (A) Phantom image of 40 and 10 nmol of [Tb(DO2Apic)-DUPA] and [Eu(DO2Aphen)-DUPA]<sup>+</sup> in the presence of 20  $\mu$ Ci Na<sup>18</sup>F. (B) Samples shown in (A) overlaid with 2 mm tissue sample (muscle) demonstrating detectable emission for 40 and 10 nmol of [Eu(DO2Aphen)DUPA]<sup>+</sup>. (C) In vivo optical imaging of 22  $\mu$ Ci [<sup>18</sup>F]-FDG and 40 nmol [Eu(DO2Aphen)-DUPA]<sup>+</sup> probe at 8 min following intratumoral administration. (D) Excised tumors imaged at 1 and 3 h postinjection (p.i.) demonstrate the persistent, detectable emission signal of [Eu(DO2Aphen)-DUPA]<sup>+</sup>. Tissue digestion and subsequent quantitation of residual Eu(III) indicate retention of 53% ID/g of the administered probe.

(PSMA),<sup>39</sup> which is highly overexpressed in metastasizing prostate cancer cells<sup>40</sup> and serves as an ideal initial proof-ofconcept targeting vector. A variety of PSMA targeting fluorophores have been studied in preclinical animal models. 41-43 The functionalized ligand, (DO2Aphen)-DUPA), was synthesized stepwise from the tert-butyl protected DO2Aphen ligand (Scheme benzylbromoacetate arm was installed under stepwise alkylation however, conditions; the subsequent debenzylation of the orthogonally protected carboxylic acid proved difficult, as under even mild conditions, significant concomitant loss of the phenanthroline antenna occurred. Mixtures of unreacted starting material, the expected product, and material lacking the antenna while still retaining the benzyl arm were produced. Though these products could be easily separated by HPLC purification, the overall yield of desired product was significantly reduced. The orthogonally protected ligand was then amidated with the tert-butyl protected form of aminopentyl-functionalized DUPA (Scheme S3).34 The ligand was deprotected and complexed as described above to afford a functionalized molecule, [Eu(DO2Aphen)-DUPA]<sup>+</sup>. The corresponding complex was characterized for its photophysical properties and exhibited a slight decrease in quantum yield, ( $\Phi_{Ln} = 10\%$ , Table 1) despite confirmation of a q = 0 complex. Likely through steric bulk or direct coordination of the amide, the coordination environment excludes the coordination of a water molecule.

As a corresponding Tb(III)-based probe, we capitalized on established chemical synthesis and characterization to produce [Tb(DO2Apic)-DUPA]. The corresponding functionalized version of the ligand had been successfully synthesized and characterized in the context of imaging with lanthanum isotopes. We pursued the previously reported synthetic approach to produce the corresponding Tb(III) complex, which produced a quantum yield  $\Phi_{Tb} = 38\%$  and retained the ability to exclude inner sphere hydration in accordance with the nonfunctionalized parent Tb(III) complex.

Following synthesis and photophysical characterization (Table 1), we conducted a multiplex imaging experiment in direct analogy with the nonfunctionalized compounds and found that discernible wavelength-selective luminescence emission using 570 or 620 nm bandpass filters was retained (Figure S65).

In Vitro and in Vivo Optical Imaging for Targeted Complexes. With PSMA-targeting constructs in hand, we sought to investigate the potential of these compounds to be utilized as optical probes in vivo. We posited that [ $^{18}$ F]-FDG, a PET imaging agent targeting GLUT-1, overexpressed in most cancer subtypes, may be ideally suited to serve as an in situ CRET source (Figure 1). First, we determined the ability of [Tb(DO2Apic)-DUPA] and [Eu(DO2Aphen)-DUPA]+ to produce luminescence emission that exhibits tissue penetration. Figure 5A and Figure 5B show phantoms imaged before (A) and after (B) the introduction of a 2 mm muscle tissue slice. Compound quantities were selected in accordance with the previously determined LODs, and 20  $\mu$ Ci of Na $^{18}$ F was employed as a CRET only reference and

as an in situ excitation source for all samples. As visible in Figure 5B, both [Eu(DO2Aphen)-DUPA]<sup>+</sup> samples (10 and 40 nmol) provide detectable emission, while the CRET only and Tb(III)mediated signal is efficiently attenuated by tissue. The emission of the Tb(III) complex is predominantly green ( $\lambda_{em} = 490, 545$  nm) and thus attenuated more strongly. Additionally, we hypothesize that the comparably low  $\Phi_{Ln}$  quantum yield of <40% may also contribute to failure to detect the corresponding emission.

Efficient tissue penetration of red-emissive Eu complexes motivated evaluation of CRET-mediated excitation of the targeted [Eu(DO2Aphen)-DUPA]<sup>+</sup> in a murine xenograft PSMA-expressing tumor model. To closely control administered activity and optical probe, we chose intratumoral administration of either only 22 µCi [18F]-FDG or 40 nmol of [Eu(DO2Aphen)-DUPA]+ coadministered with 22 µCi [18F]-FDG. Mice were subsequently imaged at 8 min postinjection (Figure 5C), followed by tumor resection and ex vivo imaging of the two masses at 1 and 3 h postinjection (Figure 5D). Both in vivo and ex vivo images demonstrate detectable luminescence emission by the [Eu(DO2Aphen)DUPA]+ construct, even after prolonged exposure, partial radioactive decay, and clearance of the Eu(III) probe. Inductively coupled plasma optical emission spectroscopy (ICP-OES) revealed that the tumor had retained 0.78 nmol of Eu(III) probe, yet ex vivo imaging in the presence of 27 µCi and 13 µCi of [18F]-FDG provided excellent tumor conspicuity, indicating that prospective, systemic administration of detectable Eu(III) probe doses is feasible. We currently cautiously hypothesize that an increased blue light emission of tissue (n > 1.35) with a refractive index greater than water (n = 1.33) is responsible for the detectability of the Eu(III) emission in vivo. Experiments to investigate this effect are ongoing.



## CONCLUSIONS

The magnetic and optical properties of discrete lanthanide complexes provide unique opportunities for bioimaging applications. Undoubtedly, Gd(III)- or Eu(II)-based magnetic resonance imaging (MRI) has long been considered the most compatible with targeted in vivo imaging using discrete molecular complexes. In vivo optical imaging, while conceptually feasible as lanthanides Eu(III), Sm(III), Tm(III), Ho(III), Yb(III), and Nd(III) emit in the NIR optical window, has remained underexplored due to inherently low  $\Phi_{Ln}$  and/or indirect means of excitation which require tissue-impermeable, short wavelength excitation.

Here, we show for the first time that in situ excitation of discrete Tb(III) and Eu(III) complexes using Na<sup>18</sup>F as a CRET source enables multiplex imaging using conventional optical imaging equipment. Optical imaging of Tb(III) or Eu(III) phantoms in the presence of a CRET source is possible at concentrations as low as 4 nmol (20  $\mu$ M) and in vivo optical imaging as low as 10 nmol (50  $\mu$ M) with Eu(III). Of note, this represents an order of magnitude lower probe

concentration as what is typically required for Gd(III)-enhanced MRI imaging  $^{44-46}$  or for organic sensor probes.  $^{47-50}$  The required probe concentration can be further lowered by enhancing the quantum yield  $\Phi_{Ln}$ , especially for Eu(III) probes, further decreasing the limit of detection by at least 1 order of magnitude, in line with targeted, organic optical probes.  $^{51-53}$  Efforts to enhance  $\Phi_{Eu}$  of conjugated Eu(III) complexes while retaining aqueous solubility and devising means to systemically administer both the CRET source and lanthanide probe to illuminate cancer targets in an orthotopic tumor model are currently ongoing.

Lastly, we highlight that our work unlocks targeted, luminescent lanthanide coordination complexes as a to-date untapped compound class with potential for in vivo optical imaging.



## **EXPERIMENTAL SECTION**

All starting materials were purchased from Acros Organics, Alfa Aesar, Macrocyclics, Sigma-Aldrich, or TCI America and used without further purification. NMR spectra (<sup>1</sup>H, <sup>13</sup>C) were collected on a 700 MHz Advance III Bruker, 500 MHz, or 400 MHz Bruker instrument at 25 °C and processed using TopSpin 4.0.7. Chemical shifts are reported as parts per million (ppm). Low-resolution electrospray ionization (ESI) mass spectrometry and highresolution (ESI) mass spectrometry were carried out at the Stony Brook University Center for Advanced Study of Drug Action (CASDA) with a Bruker Impact II UHR QTOF MS system. UV-vis spectra were collected with the NanoDrop 1C instrument (AZY1706045). Spectra were recorded from 190 to 850 nm in a quartz cuvette with 1 cm path length. Luminescence measurements were carried out on a Hitachi F-7100 FL spectrophotometer. Wavelength scans were collected by exciting at the appropriate wavelength (283 nm for Eu(III) and 282 for Tb(III)) for antennamediated excitation and minimization of scattering interference. Emission spectra were collected from 300 to 800 nm, with 1.0 nm excitation and 5.0 nm emission slit widths, 1200 s scan time, 0.05 s response time, and PMT voltage = 400 V. Quantum yield measurements for europium were carried out using Ru(bipy)3 as standard ( $\lambda_{ex} = 450$  nm). Terbium quantum yield measurements used [Tb(DO3Apic)]- (QY= 47%) as a standard. Lifetime measurements were executed using the following settings: scan time 20 ms; chopping speed of 40 Hz; excitation wavelength of 255.0 nm (with the exception of [Eu(DO2Aphen)]+ which was excited at 285.0 nm) and emission wavelength of 555.0 nm; 0 s delay; excitation and emission slit widths of 10 nm each; 0.5 s response. Complexes were dissolved in H<sub>2</sub>O or D<sub>2</sub>O, and samples were resuspended and lyophilized in D2O repeatedly prior to measurement. A quartz cuvette with a 1 cm path length was used. ICP-OES was carried out using an Agilent 5110 inductively coupled plasma optical emission spectrometer. A 10-point standard curve or a 6-point standard curve with a check standard with respect to europium or terbium was used, and fits were found to be at least R<sup>2</sup> of 0.999. Concentrations were then back calculated to the stock sample concentration. IVIS Lumina series III from Caliper LifeSciences small animal imager was used for imaging. All scans were collected with blocked excitation and either open emission filter or selected emission filters as discussed. The open emission filter runs from 500 to 875 nm, with an average bandwidth of 20 nm and a collection time of 5 min. Images were analyzed with Living Image software (version 4.3.1). Preparative HPLC was carried out using a Shimadzu HPLC-20AR equipped with a binary gradient, pump, UV- vis detector, manual injector on a Phenomenex Luna C18 column (250 mm × 21.2 mm, 100 Å, AXIA packed). Method A (preparative purification method): A = 0.1% TFA in water, B =0.1% TFA in MeCN. Gradient, 0-5 min: 95% A. 5-24 min: 5-95% B gradient. Analytical reversed phase HPLC of compounds was performed with a Shimadzu system, equipped with a CBM-20A interface, SIL-20A HT autosampler, SPD-20AV UV detector, LabLogic dual scan-RAM radio-HPLC detector, and a LC-20AB pump. A reversed-phase C18 column (Phenomenex Luna 5 µm  $C_{18}(2)$  100 Å, LC column 150 mm × 3 mm) was used for analytical purposes. The mobile phase consisted of 0.1% TFA in deionized water (A) and 0.1% TFA acetonitrile (B). A gradient of solvent B (5-95% over 20 min) at a flow rate of 0.8 mL/min was used for analytical characterization runs (method C).

Synthesis of [Eu(DO2Aphen)-DUPA]\*. Benzyl{7-[(6-methyl-4,5diaza-3-phenanthryl)methyl]-4,10-bis(tert-

butoxycarbonylmethyl)1,4,7,10-tetraaza-1-cyclododecyl}acetate (7). Benzyl bromoacetate (2.9 μL, 0.018 mmol), 6 (7.4 mg, 0.012 mmol), and K<sub>2</sub>CO<sub>3</sub> (16.9 mg, 0.122 mmol) were combined in dry MeCN (5 mL) and refluxed overnight. K2CO3 was filtered out, and the filtrate was concentrated. The resulting residue was purified using reverse phase preparative HPLC (method A) with pure product eluting at 16.6 min. Fractions containing product were pooled and solvent was removed in vacuo to afford pure 7 (4.7 mg, 51% yield). <sup>1</sup>H NMR (CD<sub>3</sub>OD, 700 MHz): δ 9.06 (br s, 1H), 8.24 (m, 5H), 7.44 (m, 5H), 5.36 (s, 2H), 5.19, 4.16 (s, 2H), 4.03-3.33 (m, 16H), 3.30-3.02 (m, 16H), 3.19 (s, 3H), 1.40 (s, 18H).  ${}^{13}C\{{}^{1}H\}$ NMR (CD<sub>3</sub>OD, 175 MHz): δ 174.2, 167.5, 159.5, 139.5, 137.3, 136.4, 130.7, 129.9, 129.6, 129.5, 129.3, 127.9, 127.9, 86.7, 84.0, 69.1, 67.5, 61.1, 60.1, 55.6, 49.8, 28.4, 21.6. ESI- MS calcd for  $C_{43}H_{58}N_6O_6$ : 754.44. Found: 755.4 [M + H]<sup>+</sup> and 378.3 [M + 2H]<sup>2+</sup>.

{7-[(6-Methyl-4,5-diaza-3-phenanthryl)methyl]-4,10-bis(tertbutoxycarbonylmethyl)-1,4,7,10-tetraaza-1-cyclododecyl}acetic Acid (8). To a solution of 7 (16.6 mg, 0.022 mmol) in MeOH (5 mL), a suspension of Pd/C (1.2 mg, 7% w/w) in MeOH (1 mL) was added. The flask was evacuated and charged with H<sub>2</sub> (1 atm), and then the mixture was stirred at room temperature for 5 h. The reaction mixture was filtered, and the solvent was removed in vacuo. The resulting oil was purified with reverse phase preparative HPLC (method A) with the product eluting at 13.6 min. The fractions containing product were combined and the solvent was removed in vacuo to afford 8 (5.4 mg, 37% yield). <sup>1</sup>H NMR (CD<sub>3</sub>OD, 700 MHz): δ 8.63 (s, 1H), 8.57 (d, 1H), 8.09 (d, 1H), 8.05 (d, 1H), 8.00 (s, 1H), 7.89 (d, 1H), 4.93 (s, 2H), 3.96-3.44 (m, 12H), 3.29-3.03 (m, 8H), 3.02 (s, 3H), 1.20 (s, 18H).  ${}^{13}C{}^{1}H{}^{1}NMR$ (175 MHz, CD<sub>3</sub>OD): δ 172.3, 160.5, 139.3, 130.5, 129.5, 129.2, 128.4, 127.6, 126.6, 126.5, 83.5, 59.4, 55.5, 55.3, 52.7, 50.4, 49.5, 28.3, 24.2. ESI-MS calcd for C<sub>36</sub>H<sub>52</sub>N<sub>6</sub>O<sub>6</sub>: 664.39. Found:  $665.4 [M + H]^+$  and  $333.4 [M + 2H]^{2+}$ .

Di-tert-butyl 2-(3-{4-[5-(2-{7-[(6-methyl-4,5-diaza-3-phenanthryl)methyl]-4,10-bis(tert-butoxycarbonylmethyl)-1,4,7,10-tetraaza-1c y c l o d o d e c y l } a c e t y l a m i n o ) p e n t y l a m i n o ] - 4 - o x o - 1 - t e r t butoxycarbonylbutyl}ureido)glutarate (9). 8 (1.5 mg, 0.002 mmol) was added to a solution of DIPEA (0.45  $\mu L,\ 0.027$  mmol) and HBTU (1.3 mg, 0.003 mmol) in DMF (5 mL). The mixture was allowed to stir for 15 min, and then a solution of di-tert-butyl (R)-

2-(3-((R)-4-(5aminopentylamino)-4-oxo-1-tert-

butoxycarbonylbutyl)ureido)glutarate<sup>34</sup> (1.3 mg, 0.002 mmol) in DMF (2 mL) was added. The reaction was stirred overnight at room temperature, and the solvent was then removed in vacuo. The crude product was purified using reverse phase preparative HPLC (method A) with the product eluting at 19.2 min (1.6 mg, 58% yield).  $^{1}$ H NMR (CD<sub>3</sub>OD, 700 MHz):  $\delta$ 

 $8.71~(s,\,1H),\,8.61~(s,\,1H),\,8.24~(s,\,1H),\,8.12~(q,\,2H),\,7.95~(s,\,1H),\,5.02~(s,\,2H),\,4.22~(m,\,1H),\,4.15~(m,\,1H),\,3.98~(s,\,2H),\,3.93–2.91~(m,\,20H),\,3.67~(s,\,4H),\,3.19~(m,\,4H),\,3.06~(s,\,3H),\,2.28~(m,\,4H),\,2.08~(m,\,2H),\,1.84~(m,\,2H),\,1.50~(m,\,4H),\,1.49,\,1.47,\,1.32~(s,\,45H),\,1.38~(m,\,2H).$  ESI-MS calcd for  $C_{64}H_{102}N_{10}O_{13}$ : 1218.76. Found: 1219.8  $[M+H]^+$  and 610.6  $[M+2H^+]^{2+}$ .

2-(3-{4-[5-(2-{4,10-Bis(carboxymethyl)-7-[(6-methyl-4,5-diaza-3phenanthryl)methyl]-1,4,7,10-tetraaza-1-

cyclododecyl}acetylamino)pentylamino]-1-carboxy-4-

oxobutyl}ureido)glutaric Acid ((DO2Aphen)DUPA). 9 (1.6 mg, 0.001 mmol) was dissolved in a solution of 1:2 DCM/TFA (1.5 mL) and stirred at room temperature overnight. The solvent was removed in vacuo, and the product was redissolved in H<sub>2</sub>O. The solution was then lyophilized to yield (DO2Aphen)-DUPA as a white solid (0.8 mg, 65% yield).  $^{1}$ H NMR (CD<sub>3</sub>OD, 700 MHz):  $\delta$  8.98 (d, 1H), 8.70 (s, 1H), 8.22 (q, 2H), 8.12 (d, 2H), 4.97 (s, 2H), 4.27 (q, 1H), 4.23 (q, 1H), 4.02 (br s, 2H), 3.66–3.05 (m, 16H), 3.51 (m, 4H) 3.16 (s, 3H), 2.38 (m, 2H), 2.31 (m, 2H), 2.16 (m, 2H), 2.11 (m, 2H), 1.86 (m, 4H), 1.59 (m, 4H), 1.42 (m, 2H). HRMS calcd for  $C_{44}H_{62}N_{10}O_{13}$ : 938.4498. Found: 939.4560. HPLC:  $t_R$  = 6.3 min (method C).

Synthesis and Characterization of Eu Complexes. To a solution

of ligand dissolved in water, 1 equiv of Eu(OTf)3 salt was added. The pH was adjusted to 7.0-7.5 using 0.1 M NaOH. The complex was then purified via SepPak (Waters Sep-Pak C18 Plus short cartridge, 360 mg sorbent per cartridge, 55-105 µm particle size). The fractions containing product were pooled and lyophilized, yielding white solids. [Eu(DO3Aphen)] product eluted in 90:10 (H<sub>2</sub>O/MeCN). HRMS calcd for C<sub>28</sub>H<sub>33</sub>EuN<sub>6</sub>O<sub>6</sub>: 702.1674, 700.1660. Found: 723.1546  $[M + Na]^+$ .  $R_t = 5.7 \text{ min (method C)}$ . [Eu(DO2Aphen)]<sup>+</sup> product eluted in 90:10 (H<sub>2</sub>O/MeCN). HRMS calcd for  $C_{26}H_{31}EuN_6O_4$ : 644.1619. Found: 643.1675 and 645.1692  $[M + H]^+$ .  $R_t = 5.7 \text{ min (method C)}$ .  $[Eu(DO2Aphen)-DUPA]^+$ product eluted in 90:10 (H<sub>2</sub>O/MeCN). HRMS calcd for C<sub>44</sub>H<sub>59</sub>EuN<sub>10</sub>O<sub>13</sub>: 1089.3554. Found: 1087.3538 and 1089.3558 [M + H]<sup>+</sup>.  $R_t = 6.3$  min (method C). The kinetic inertness of [Eu(DO3Aphen)] and [Tb(DO3Apic)] was investigated with a diethylenetriaminepentaacetic acid (DTPA) challenge. The complexes in 1× DPBS (pH 7.4) [(Eu(DO3Aphen)], 1.85 mM, 20 μL; [Tb(DO3Apic)]-, 0.48 mM, 230 μL) were combined with 1000× excess DTPA ([Eu(DO3Aphen)], 75 mM, 492 µL; [Tb-(DO3Apic)]-, 150 mM, 741 µL) and excess buffer (total volume of each sample, 2 mL), and the UV-vis spectrum and analytical HPLC trace were recorded over 14 days. UV-vis spectra were collected with the NanoDrop <sup>1</sup>C instrument (AZY1706045), and spectra were recorded from 190 to 850 nm in a quartz cuvette with 1 cm path length. For [Eu(DO3Aphen)] absorbance maximum at 285 nm is characteristic for the complex and at 275 nm it is characteristic of the unchelated ligand. The retention times of the complex and uncomplex ligands were 5.02 and 4.85 min, respectively. For [Tb(DO3Apic)] absorbance maximum at 275 nm is characteristic

for the complex and at 268 nm it is characteristic of the unchelated ligand. The retention times of the complex and uncomplex ligands were 1.55 and 1.52 min, respectively. UV-vis measurements were collected daily, and HPLC analysis was conducted every 48 h with

a standard of complex and free ligand run alongside the challenge samples.

Phantom Preparation, Imaging, and Image Processing. Concentrations of each lanthanide complex were diluted, and 200  $\mu L$  aliquots of dilutions were prepared in 1× DPBS buffer to which  $10~\mu L$  of  $Na^{18}F$  (10 or  $20~\mu Ci$ ) was added to produce a final volume of  $210~\mu L$  IVIS Lumina series III from Caliper LifeSciences small animal imager was used for imaging. All scans were collected with blocked excitation and either open emission filter or selected emission filters as discussed. The open emission filter measures from 500 to 875 nm, with an average bandwidth of 20 nm and a collection time of 5 min. Images were analyzed with Living Image software (version 4.3.1). Regions of interest (ROI) were determined in triplicate with the ROI tool for each concentration. Radiance values for each complex are subtracted from the Cherenkov-only sample (Na^{18}F in 1× DPBS buffer).

In Vitro and in Vivo Imaging. To assess the quenching effects of tissue, phantom images of  $[Eu(DO2Aphen)\text{-}DUPA]^+$  and [Tb(DO2Apic)-DUPA] were collected in the presence of 2 mm turkey slices. Solutions of 10 and 40 nmol of  $[Eu(DO2Aphen)\text{-}DUPA]^+$  and [Tb(DO2Apic)-DUPA] in 1× DPBS were doped with 20  $\mu\text{Ci}$  of  $Na^{18}\text{F}$  and imaged. Turkey slices (2 mm thickness) were layered on top of the phantoms, and the samples were reimaged. All animal experiments and procedures were performed in accordance with the National Institutes of Health's "Guide for the Care and Use of

Laboratory Animals" and approved by Institutional Animal Care and Use Committee (IACUC) at Stony Brook Medicine. Male Ncr mice (Taconic Biosciences, Rensselaer, NY) were inoculated subcutaneously on the right and left shoulders with  $1.0 \times 10^6 PSMA$ positive PC-3 PIP cells suspended in Matrigel (1:2 DPBS/Matrigel). When the tumors reached a suitable size, mice were anesthetized with isoflurane and a mixture of [Eu(DO2Aphen)-DUPA] $^+$ (40 nmol) and [ $^{18}$ F]-FDG (100 or 22  $\mu$ Ci, NCM-USA, Bronx, NY) was injected intratumorally to the right shoulder. A corresponding volume and activity of saline and [18F]-FDG (100 or 22 µCi) were injected intratumorally to the left shoulder. Mice were imaged at 5 min (100  $\mu$ Ci) and 8 min (22  $\mu$ Ci) p.i. with the IVIS Lumina series III small animal imager. Mice were sacrificed 3 h p.i. (100 µCi dose) and 1 h p.i. (22 µCi dose), and tumors were extracted and imaged. Tumors were digested with concentrated nitric acid, diluted, and remaining Eu content was determined by ICP-OES.



## ASSOCIATED CONTENT

## \* Supporting Information

The Supporting Information is available free of charge at https://pubs.acs.org/doi/10.1021/jacs.1c04264.

Experimental procedures; NMR, HRMS, and HPLC results; characterization of complexes, and fluorescence imaging results (PDF)



## **AUTHOR INFORMATION**

### Corresponding Author

Eszter Boros – Department of Chemistry, Stony Brook University, Stony Brook, New York 11794, United States; o orcid.org/0000-0002-4186-6586; Email:

eszter.boros@ stonybrook.edu

### **Authors**

Kirsten E. Martin – Department of Chemistry, Stony Brook University, Stony Brook, New York 11794, United States

Alexia G. Cosby – Department of Chemistry, Stony Brook University, Stony Brook, New York 11794, United States; orcid.org/0000-0002-2222-3497

Complete contact information is available at: https://pubs.acs.org/10.1021/jacs.1c04264

#### **Funding**

E.B. acknowledges funding sources, specifically the NIH for a NIBIB R21 Trailblazer Award (Grant R21EB030071-01A1) and the National Science Foundation for an NSF CAREER (Grant CHE 1942434). K.E.M. acknowledges support through the SBU Chemistry-Biology Interface Training Program (Grants T32 GM092714 and T32 GM136572)

## Notes

The authors declare no competing financial interest.



## **REFERENCES**

- (1) Moore, E. G.; Samuel, A. P. S.; Raymond, K. N. From Antenna to Assay: Lessons Learned in Lanthanide Luminescence. Acc. Chem. Res. 2009, 42 (4), 542–552.
- (2) Bünzli, J.-C. G. Lanthanide luminescence for biomedical analyses and imaging. Chem. Rev. 2010, 110 (5), 2729–2755.
- (3) Petoud, S.; Cohen, S. M.; Bünzli, J.-C. G.; Raymond, K. N. Stable lanthanide luminescence agents highly emissive in aqueous solution: multidentate 2-hydroxyisophthalamide complexes of Sm3+, Eu3+, Tb3+, Dy3+. J. Am. Chem. Soc. 2003, 125 (44), 13324–13325.
- (4) Xu, J.; Corneillie, T. M.; Moore, E. G.; Law, G.-L.; Butlin, N. G.; Raymond, K. N. Octadentate cages of Tb (III) 2-hydroxyisophthalamides: a new standard for luminescent lanthanide labels. J. Am. Chem. Soc. 2011, 133 (49), 19900–19910.
- (5) Xiong, R.; Mara, D.; Liu, J.; Van Deun, R.; Borbas, K. E. Excitation- and Emission-Wavelength-Based Multiplex Spectroscopy Using Red-Absorbing Near-Infrared-Emitting Lanthanide Complexes. J. Am. Chem. Soc. 2018, 140 (35), 10975–10979.
- (6) Hamon, N.; Roux, A.; Beyler, M.; Mulatier, J.-C.; Andraud, C.; Nguyen, C.; Maynadier, M.; Bettache, N.; Duperray, A.; Grichine, A.; Brasselet, S.; Gary-Bobo, M.; Maury, O.; Tripier,

- R. Pyclen-Based Ln(III) Complexes as Highly Luminescent Bioprobes for In Vitro and In Vivo One- and Two-Photon Bioimaging Applications. J. Am. Chem. Soc. 2020, 142 (22), 10184–10197.
- (7) Heffern, M. C.; Matosziuk, L. M.; Meade, T. J. Lanthanide probes for bioresponsive imaging. Chem. Rev. 2014, 114 (8), 4496–4539.
- (8) Junker, A. K. R.; Hill, L. R.; Thompson, A. L.; Faulkner, S.; Sørensen, T. J. Shining light on the antenna chromophore in lanthanide based dyes. Dalton Trans. 2018, 47 (14), 4794–4803.
- (9) Jelley, J. V. Cerenkov radiation and its applications. Br. J. Appl. Phys. 1955, 6, 227.
- (10) Thorek, D. L.; Riedl, C. C.; Grimm, J. Clinical Cerenkov luminescence imaging of 18F-FDG. J. Nucl. Med. 2014, 55 (1), 95–98.
- (11) Roda, A.; Pasini, P.; Mirasoli, M.; Michelini, E.; Guardigli, M. Biotechnological applications of bioluminescence and chemiluminescence. Trends Biotechnol. 2004, 22 (6), 295–303.
- (12) Dothager, R. S.; Goiffon, R. J.; Jackson, E.; Harpstrite, S.; Piwnica-Worms, D. Cerenkov radiation energy transfer (CRET) imaging: A novel method for optical imaging of PET isotopes in biological systems. PLoS One 2010, 5 (10), No. e13300.
- (13) Ma, X.; Kang, F.; Xu, F.; Feng, A.; Zhao, Y.; Lu, T.; Yang, W.; Wang, Z.; Lin, M.; Wang, J. Enhancement of Cerenkov Luminescence Imaging by Dual Excitation of Er<sup>3+</sup>, Yb<sup>3+</sup>-Doped Rare-Earth Microparticles. PLoS One 2013, 8 (10), e77926.
- (14) Kotagiri, N.; Niedzwiedzki, D. M.; Ohara, K.; Achilefu, S. Activatable probes based on distance-dependent luminescence associated with cerenkov radiation. Angew. Chem., Int. Ed. 2013, 52 (30), 7756–7760.
- (15) Cosby, A. G.; Ahn, S. H.; Boros, E. Cherenkov RadiationMediated In Situ Excitation of Discrete Luminescent Lanthanide Complexes. Angew. Chem., Int. Ed. 2018, 57 (47), 15496–15499.
- (16) Cosby, A. G.; Quevedo, G.; Boros, E. A High-Throughput Method To Measure Relative Quantum Yield of Lanthanide Complexes for Bioimaging. Inorg. Chem. 2019, 58, 10611–10615.
- (17) Li, H.; Tan, M.; Wang, X.; Li, F.; Zhang, Y.; Zhao, L.; Yang, C.; Chen, G. Temporal Multiplexed in Vivo Upconversion Imaging. J. Am. Chem. Soc. 2020, 142 (4), 2023–2030.
- (18) Sun, X.; Huang, X.; Guo, J.; Zhu, W.; Ding, Y.; Niu, G.; Wang, A.; Kiesewetter, D. O.; Wang, Z. L.; Sun, S.; Chen, X. Self-illuminating 64Cu-doped CdSe/ZnS nanocrystals for in vivo tumor imaging. J. Am. Chem. Soc. 2014, 136 (5), 1706–9.
- (19) Ni, D.; Ferreira, C. A.; Barnhart, T. E.; Quach, V.; Yu, B.; Jiang, D.; Wei, W.; Liu, H.; Engle, J. W.; Hu, P.; Cai, W. Magnetic Targeting of Nanotheranostics Enhances Cerenkov Radiation-Induced Photodynamic Therapy. J. Am. Chem. Soc. 2018, 140 (44), 14971–14979.
- (20) Hamon, N.; Roux, A.; Beyler, M.; Mulatier, J. C.; Andraud, C.; Nguyen, C.; Maynadier, M.; Bettache, N.; Duperray, A.; Grichine, A.; Brasselet, S.; Gary-Bobo, M.; Maury, O.; Tripier, R. Pyclen-Based Ln(III) Complexes as Highly Luminescent Bioprobes for In Vitro and In Vivo One- and Two-Photon Bioimaging Applications. J. Am. Chem. Soc. 2020, 142 (22), 10184–10197.
- (21) McMahon, B. K.; Pal, R.; Parker, D. A bright and responsive europium probe for determination of pH change within the endoplasmic reticulum of living cells. Chem. Commun. 2013, 49, 5363–5365.

- (22) Walton, J. W.; Bourdolle, A.; Butler, S. J.; Soulie, M.; Delbianco, M.; McMahon, B. K.; Pal, R.; Puschmann, H.; Zwier, J. M.; Lamarque, L.; Maury, O.; Andraud, C.; Parker, D. Very bright europium complexes that stain cellular mitochondria. Chem. Commun. 2013, 49 (16), 1600–2.
- (23) Butler, S. J.; Delbianco, M.; Lamarque, L.; McMahon, B. K.; Neil, E. R.; Pal, R.; Parker, D.; Walton, J. W.; Zwier, J. M. EuroTracker(R) dyes: design, synthesis, structure and photophysical properties of very bright europium complexes and their use in bioassays and cellular optical imaging. Dalton Trans. 2015, 44 (11), 4791–803.
- (24) Frawley, A. T.; Linford, H. V.; Starck, M.; Pal, R.; Parker, D. Enantioselective cellular localisation of europium(III) coordination complexes. Chem. Sci. 2018, 9 (4), 1042–1049.
- (25) Latva, M.; Takalo, H.; Mukkala, V. M.; Matachescu, C.; Rodríguez-Ubis, J. C.; Kankare, J. Correlation between the lowest triplet state energy level of the ligand and lanthanide(III) luminescence quantum yield. J. Lumin. 1997, 75 (2), 149–169.
- (26) Quici, S.; Gianolio, E.; Anelli, P. L.; Accorsi, G.; Botta, M.; Marzanni, G.; Armaroli, N.; Cavazzini, M.; Barigelletti, F. Highly Luminescent Eu 3+ and Tb 3+ Macrocyclic Complexes Bearing an Appended Phenanthroline Chromophore. Inorg. Chem. 2002, 41 (10), 2777–2784.
- (27) Beeby, A.; Parker, D.; de Sousa, A. S.; Clarkson, I. M.; Woods, M.; Faulkner, S.; Dickins, R. S.; Royle, L.; Williams, J. A. G. Nonradiative deactivation of the excited states of europium, terbium and ytterbium complexes by proximate energy-matched OH, NH and CH oscillators: an improved luminescence method for establishing solution hydration states. J. Chem. Soc., Perkin Trans. 2 1999, 2 (3), 493–504.
- (28) Newkome, G. R.; Theriot, K. J.; Gupta, V. K.; Fronczek, F. R.; Baker, G. R. Chemistry of heterocyclic compounds. 124. Mono- $\alpha$ functionalization of 2,9-dimethyl-l,10-Phenanthroline. J. Org. Chem. 1989, 54 (7), 1766–1769.
- (29) Kikuchi, K.; Sugihara, F.; Mizukami, S.; Yoshioka, Y.; Matsushita, H.; Nakamura, T. Activatable 19 F MRI Nanoparticle Probes for the Detection of Reducing Environments. Angew. Chem., Int. Ed. 2015, 54 (3), 1007–1010.
- (30) Lim, N.-H.; Ding-Pfennigdorff, D.; Nagase, H.; Hu, H.-Y.; Wendt, K. U.; Schultz, C.; Plettenburg, O.; Saas, J.; Nazare, M.; Ritzeler, O. DOTAM Derivatives as Active Cartilage-Targeting Drug Carriers for the Treatment of Osteoarthritis. Bioconjugate Chem. 2015, 26 (3), 383–388.
- (31) Brouwer, A. M. Standards for photoluminescence quantum yield measurements in solution (IUPAC Technical Report). Pure Appl. Chem. 2011, 83 (12), 2213–2228.
- (32) Van Houten, J.; Watts, R. J. The Effect of Ligand and Solvent Deuteration on the Excited State Properties of the Tris(2,2'bipyridyl)ruthenium(II) Ion in Aqueous Solution. Evidence for Electron Transfer to Solvent. J. Am. Chem. Soc. 1975, 97 (13), 3843–3844.
- (33) Thiele, N. A.; Woods, J. J.; Wilson, J. J. Implementing f-Block Metal Ions in Medicine: Tuning the Size Selectivity of Expanded Macrocycles. Inorg. Chem. 2019, 58 (16), 10483–10500.
- (34) Aluicio-Sarduy, E.; Thiele, N. A.; Martin, K. E.; Vaughn, B. A.; Devaraj, J.; Olson, A. P.; Barnhart, T. E.; Wilson, J. J.; Boros, E.; Engle, J. W. Establishing Radiolanthanum Chemistry for Targeted Nuclear Medicine Applications. Chem. Eur. J. 2020, 26 (6), 1238–1242.
- (35) Thiele, N. A.; Brown, V.; Kelly, J. M.; Amor-Coarasa, A.; Jermilova, U.; MacMillan, S. N.; Nikolopoulou, A.; Ponnala, S.; Ramogida, C. F.; Robertson, A. K. H.; Rodríguez-Rodríguez,

- C.; Schaffer, P.; Williams, C., Jr; Babich, J. W.; Radchenko, V.; Wilson, J. J. An Eighteen-Membered Macrocyclic Ligand for Actinium-225 Targeted Alpha Therapy. Angew. Chem., Int. Ed. 2017, 56 (46), 14712–14717.
- (36) Meimetis, L. G.; Boros, E.; Carlson, J. C.; Ran, C.; Caravan, P.; Weissleder, R. Bioorthogonal Fluorophore Linked DFO Technology Enabling Facile Chelator Quantification and Multimodal Imaging of Antibodies. Bioconjugate Chem. 2016, 27 (1), 257–263.
- (37) Adams, C. J.; Wilson, J. J.; Boros, E. Multifunctional Desferrichrome Analogues as Versatile 89Zr(IV) Chelators for ImmunoPET Probe Development. Mol. Pharmaceutics 2017, 14 (8), 2831–2842.
- (38) Xu, J.; Zhou, J.; Chen, Y.; Yang, P.; Lin, J. Lanthanide-activated nanoconstructs for optical multiplexing. Coord. Chem. Rev. 2020, 415, 213328.
- (39) Kularatne, S. A.; Zhou, Z.; Yang, J.; Post, C. B.; Low, P. S. Design, Synthesis, and Preclinical Evaluation of Prostate-Specific Membrane Antigen Targeted 99m Tc-Radioimaging Agents. Mol. Pharmaceutics 2009, 6 (3), 790–800.
- (40) Ghosh, A.; Heston, W. D. W. Tumor target prostate specific membrane antigen (PSMA) and its regulation in prostate cancer. J. Cell. Biochem. 2004, 91 (3), 528–539.
- (41) Chen, Y.; Pullambhatla, M.; Banerjee, S. R.; Byun, Y.; Stathis, M.; Rojas, C.; Slusher, B. S.; Mease, R. C.; Pomper, M. G. Synthesis and Biological Evaluation of Low Molecular Weight Fluorescent Imaging Agents for the Prostate-Specific Membrane Antigen. Bioconjugate Chem. 2012, 23, 2377–2385.
- (42) Baranski, A. C.; Schäfer, M.; Bauder-Wüst, U.; Roscher, M.; Schmidt, J.; Stenau, E.; Simpfendörfer, T.; Teber, D.; Maier-Hein, L.; Hadaschik, B.; Haberkorn, U.; Eder, M.; Kopka, K. PSMA-11-Derived dual-Labeled PSMA inhibitors for preoperative PET imaging and precise fluorescence-Guided surgery of prostate cancer. J. Nucl. Med. 2018, 59 (4), 639–645.
- (43) Hensbergen, A. W.; Van Willigen, D. M.; Van Beurden, F.; Van Leeuwen, P. J.; Buckle, T.; Schottelius, M.; Maurer, T.; Wester, H. J.; Van Leeuwen, F. W. B. Image-Guided Surgery: Are We Getting the Most out of Small-Molecule Prostate-Specific-Membrane-AntigenTargeted Tracers? Bioconjugate Chem. 2020, 31 (2), 375–395.
- (44) Gale, E. M.; Jones, C. M.; Ramsay, I.; Farrar, C. T.; Caravan, P. A Janus Chelator Enables Biochemically Responsive MRI Contrast with Exceptional Dynamic Range. J. Am. Chem. Soc. 2016. 138 (49), 15861–15864.
- (45) Wang, H.; Jordan, V. C.; Ramsay, I. A.; Sojoodi, M.; Fuchs, B. C.; Tanabe, K. K.; Caravan, P.; Gale, E. M. Molecular Magnetic Resonance Imaging Using a Redox-Active Iron Complex. J. Am. Chem. Soc. 2019, 141 (14), 5916–5925.
- (46) Yu, M.; Bouley, B. S.; Xie, D.; Enriquez, J. S.; Que, E. L. (19)F PARASHIFT Probes for Magnetic Resonance Detection of H2O2 and Peroxidase Activity. J. Am. Chem. Soc. 2018, 140 (33), 10546–10552.
- (47) Abdelfattah, A. S.; Kawashima, T.; Singh, A.; Novak, O.; Liu, H.; Shuai, Y.; Huang, Y.-C.; Campagnola, L.; Seeman, S. C.; Yu, J.; Zheng, J.; Grimm, J. B.; Patel, R.; Friedrich, J.; Mensh, B. D.; Paninski, L.; Macklin, J. J.; Murphy, G. J.; Podgorski, K.; Lin, B.-J.; Chen, T.W.; Turner, G. C.; Liu, Z.; Koyama, M.; Svoboda, K.; Ahrens, M. B.; Lavis, L. D.; Schreiter, E. R. Bright and photostable chemigenetic indicators for extended in vivo voltage imaging. Science 2019, 365 (6454), 699–704.
- (48) He, S.; Li, J.; Lyu, Y.; Huang, J.; Pu, K. Near-Infrared Fluorescent Macromolecular Reporters for Real-Time Imaging and

- Urinalysis of Cancer Immunotherapy. J. Am. Chem. Soc. 2020, 142 (15), 7075–7082.
- (49) Ning, Y.; Liu, Y. W.; Yang, Z. S.; Yao, Y.; Kang, L.; Sessler, J. L.; Zhang, J. L. Split and Use: Structural Isomers for Diagnosis and Therapy. J. Am. Chem. Soc. 2020, 142 (14), 6761–6768.
- (50) Yang, Y.; Zhou, T.; Jin, M.; Zhou, K.; Liu, D.; Li, X.; Huo, F.; Li, W.; Yin, C. Thiol-Chromene "Click" Reaction Triggered SelfImmolative for NIR Visualization of Thiol Flux in Physiology and Pathology of Living Cells and Mice. J. Am. Chem. Soc. 2020, 142 (3), 1614–1620.
- (51) Ye, D.; Shuhendler, A. J.; Cui, L.; Tong, L.; Tee, S. S.; Tikhomirov, G.; Felsher, D. W.; Rao, J. Bioorthogonal cyclizationmediated in situ self-assembly of small-molecule probes for imaging caspase activity in vivo. Nat. Chem. 2014, 6 (6), 519–26.
- (52) Chen, Z.; Mu, X.; Han, Z.; Yang, S.; Zhang, C.; Guo, Z.; Bai, Y.; He, W. An Optical/Photoacoustic Dual-Modality Probe: Ratiometric in/ex Vivo Imaging for Stimulated H2S Upregulation in Mice. J. Am. Chem. Soc. 2019, 141 (45), 17973–17977.
- (53) Boss, M.; Bos, D.; Frielink, C.; Sandker, G.; Ekim, S.; Marciniak, C.; Pattou, F.; van Dam, G.; van Lith, S.; Brom, M.; Gotthardt, M.; Buitinga, M. Targeted Optical Imaging of the Glucagonlike Peptide 1 Receptor Using Exendin-4-IRDye 800CW. J. Nucl. Med. 2020, 61 (7), 1066–1071.